Korean Journal of Remote Sensing, Vol.36, No.1, 2020, pp.15~27
https://doi.org/10.7780/kjrs.2020.36.1.2

ISSN 1225-6161 (Print)
ISSN 2287-9307 (Online)

Article

Land Use Feature Extraction and Sprawl Development Prediction from Quickbird Satellite Imagery Using Dempster-Shafer and Land Transformation Model

Maryam Adel Saharkhiz[1] · Biswajeet Pradhan [2]† · Hossein Mojaddadi Rizeei[3] · Hyung-Sup Jung [4]

Abstract: Accurate knowledge of land use/land cover (LULC) features and their relative changes over upon the time are essential for sustainable urban management. Urban sprawl growth has been always also a worldwide concern that needs to carefully monitor particularly in a developing country where unplanned building constriction has been expanding at a high rate. Recently, remotely sensed imageries with a very high spatial/spectral resolution and state of the art machine learning approaches sent the urban classification and growth monitoring to a higher level. In this research, we classified the Quickbird satellite imagery by object-based image analysis of Dempster-Shafer (OBIA-DS) for the years of 2002 and 2015 at Karbala-Iraq. The real LULC changes including, residential sprawl expansion, amongst these years, were identified via change detection procedure. In accordance with extracted features of LULC and detected trend of urban pattern, the future LULC dynamic was simulated by using land transformation model (LTM) in geospatial information system (GIS) platform. Both classification and prediction stages were successfully validated using ground control points (GCPs) through accuracy assessment metric of Kappa coefficient that indicated 0.87 and 0.91 for 2002 and 2015 classification as well as 0.79 for prediction part. Detail results revealed a substantial growth in building over fifteen years that mostly replaced by agriculture and orchard field. The prediction scenario of LULC sprawl development for 2030 revealed a substantial decline in green and agriculture land as well as an extensive increment in build-up area especially at the countryside of the city without following the residential pattern standard. The proposed method helps urban decision-makers to identify the detail temporal-spatial growth pattern of highly populated cities like Karbala. Additionally, the results of this study can be considered as a probable future map in order to design enough future social services and amenities for the local inhabitants.

Key Words: Urban growth prediction, remote sensing, land transformation model, object-based image analysis, Dempster-Shafer

Received August 12, 2019; Revised August 19, 2019; Accepted September 5, 2019; Published online October 1, 2019

[1] PhD Student, The Centre for Advanced Modelling and Geospatial Information Systems (CAMGIS), University of Technology Sydney
[2] Distinguished Professor, The Centre for Advanced Modelling and Geospatial Information Systems (CAMGIS), University of Technology Sydney
[3] Postdoctoral Research Associate, The Centre for Advanced Modelling and Geospatial Information Systems (CAMGIS), University of Technology Sydney
[4] Professor, Department of Geoinformatics, University of Seoul

† Corresponding Author: Biswajeet Pradhan (biswajeet.pradhan@uts.edu.au)

1. Introduction

Appropriate urban planning accomplishment highly depends on the use of comprehensive and detail spatial data (Abdullahi *et al*., 2018); such precise data can be acquired from satellite/airborne remote sensing (RS) images (Bhatta *et al*., 2010).

Urban applications have been using satellite data for various processing, containing extraction of the urban object accurately and fast, updating of thematic maps of road networks, temporal monitoring, and land use/ land cover (LULC) mapping. Very-high-resolution (VHR) satellite images are often utilized for urban LULC classification at an ultra-fine scale due to their comprehensive information even from the complex urban scene (Rizeei and Pradhan, 2019). Since urban regions are obviously heterogeneous zones where identifying by various LULCs, high spectral and spatial satellite imageries can play a significant role to differentiate features (Rizeei *et al*., 2018). However, some urban LULC classes like road and building have shown parallel spectral reflectance with non-urban types, for example, parking lot, due to their similar physical characteristics (He *et al*., 2010). Therefore, researchers have faced many difficulties during the RS image processing of urban areas (Kumar *et al*., 2012). Recently, numerous high and very-high-resolution satellite images, such as IKONOS (1999), QuickBird (2001), GeoEye-1 (2008), Worldview-3 (2014), and SPOT-6 (2014), have been processed by several image processing techniques.

There are many studies on the negative impacts of urban sprawl expansion on social, environmental, and economic facets that specifies the necessity for controlling and monitoring of urban growth via decent strategies (Abdullahi *et al*., 2018; Dadi *et al*., 2016). Thus, assessment of the current condition and prediction of LULC changes can help managers with valuable information for coping with the consequence of urbanization (Aal-shamkhi *et al*., 2017). Variation on LULC can be detected and predicted deploying several methods, such as agent-based (Grimm *et al*., 2006), artificial neural network (Pijanowski *et al*., 2002), Markov chain (Koomen and Borsboom-van Beurden, 2011), Conversion of land use and its effects at small region extent (CLUE-S) model (Verburg *et al*., 2002), grid-based forward and backward land use change (GEOMOD) model (Pontius Jr and Chen, 2006), The SLEUTH model i.e. slope, land use, exclusion, urban extent, transportation and hill-shade (Dietzel and Clarke, 2007), statistical data-mining models (Abdullahi *et al*., 2015), and cellular automata (Li and Yeh, 2000). Beside them, Land Transformation Model (LTM) is one of the recent geospatial-based models particularly to model the large areas. LTM mostly has the capacity to align with a range of contributing parameters like environmental, socio-economic and even political matters. It has also had an ability to link LULC dynamics to ecological process, for instance, soil erosion prediction (Nampak *et al*., 2018; Rizeei *et al*., 2016) and forest canopy changes (Pijanowski *et al*., 2002). Additionally, LTM provides LULC planners on future probable environmental effects in regional and local scale (Tayyebi *et al*., 2013). However, this is a first attempt to experiment the combination of LTM with Dempster-Shafer in one of the strategic cities of Iraq called Karbala, where sustainable urban planning is a serious issue due to receiving enormous immigrant from other cities every year. Our framework has not been implemented by other researchers before, since, we applied a state-of-the-art integrated technique to classify the remotely sensed imageries deployed by object-based image analysis of Dempster-Shafer (OBIA-DS) and spatial prediction for future LULC by LTM, which enables decision-makers to have a broader view about urban growth to plan accurately. The challenge comes into attaining accurate technique to detect, monitor and predict the spatial development of urban growth. Hence, very high-resolution satellite imagery of Quickbird for two periods of times (2002 and 2015) was chosen to process for this research.

2. Dataset and Methodology

1) Study Area

The Karbala city of Iraq and its surrounded regions are chosen as the study area. This part is a significant part of Karbala city where future development would be taken the place. It situated between 32.37 N and 44.4 E with an area of almost 62 km^2 (Fig. 1). This area has multiple LULC classes including agricultural land, orchards, palms trees, and urban features and houses. Karbala is one of the important cities of Iraq where an estimated population are 1,013,500 persons in 2008.

2) Dataset

Two very-high-spatial-resolution images of Quickbird were processed in this study. These images provided detailed information of the location of study area (Table 1). They contained five spectral bands and 0.6 m spatial resolution. The first image captured on

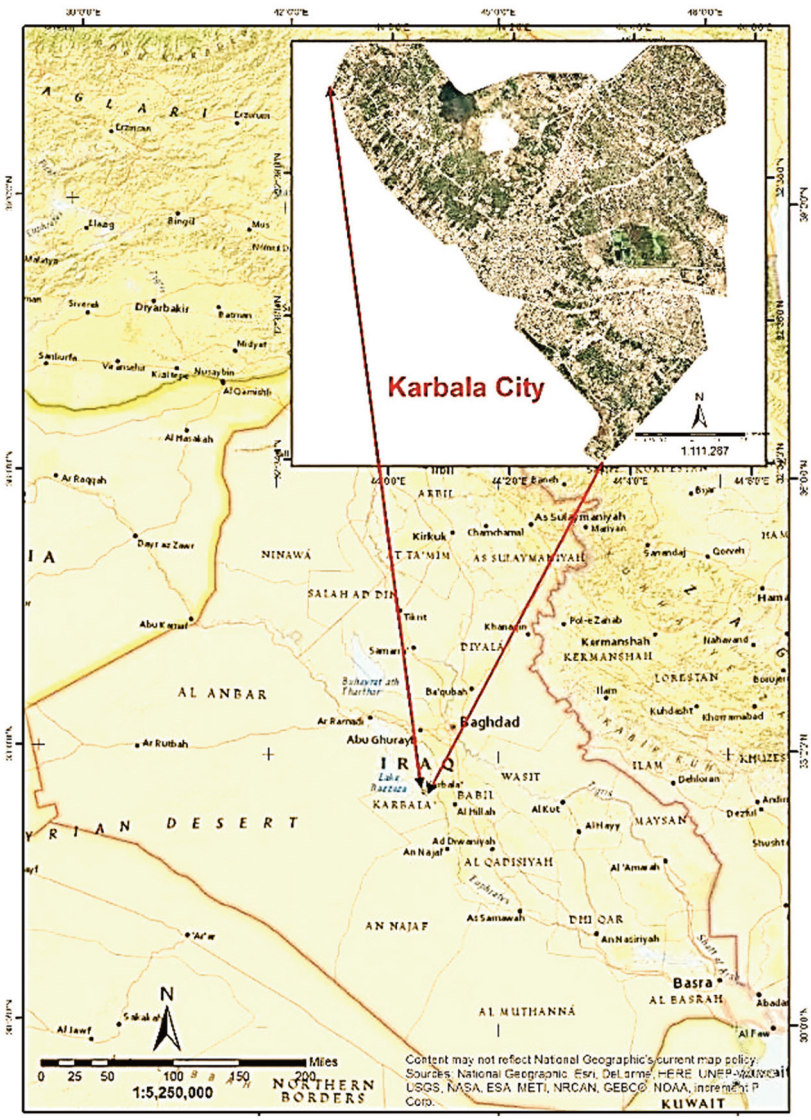

Fig. 1. Location of the study area.

Table 1. Characteristics of the Quickbird satellite image

Spatial resolution	Panchromatic	0.6 m GSD	
	Multispectral	2.4 m GSD	
Spectral resolution	445-900 nm	Blue band	450-520 nm
		Green band	520-600 nm
		Red band	630-690 nm
		Near Infrared band	760-900 nm

12th of September 2002 and the second one acquired on 7th of September 2015 from Karbala city. Both imageries were acquired on the same season in order to remove the seasonal bias for change detection assessment. For the purpose of this study, we used four spectral bands of Quickbird, inducing blue, red, green and near-infrared bands for image processing.

3) Methods

The methodological processes of this study are listed as below:

a) Correcting the geometric, radiometric, and atmospheric errors from original satellite imageries.
b) Classifying the images using object-based image analysis approach of Dempster-Shafer (OBIA-DS) and evaluate the accuracy of classified results.
c) Detecting the real changes in land use land cover from 2002 till 2015.
d) Land use change modelling: predicting the future growth and sprawl development using land transformation model (LTM).

(1) Image pre-processing

In order to remove the atmospheric errors from satellite images, Dark object subtraction method was used in Envi 5.8 software. The images then geometrically checked by 13 ground control points (GCPs) which collected from different parts of the imageries. The images were projected into universal transverse Mercator (UTM) coordinate system of zone 48 south with datum of WGS1984. In radiometric correction process, the image digital number (DN) values were converted to surface reflectance to explain the surface physical properties (Sridharan, 2012). In this study, relative radiometric correction was applied on both imageries as Equation 1 describes:

$$L = \frac{DN \times M + A}{\cos(\theta_{SZ})} \quad (1)$$

where L is the reflectance of the electromagnetic radiation in units of W/m^2/ster/μm, and A is the offset, which can be derived from the satellite metadata. M is band specific multiplicative rescaling factor from metadata. θ_{SE} is Local sun elevation angle (metadata) and θ_{SZ} is local solar zenith angle; $\theta_{SZ} = 90° - \theta_{SE}$ (i.e. gain).

(2) OBIA Image processing

① Segmentation

OBIA is an operative image processing technique to merge multiple pixel values into a single object based on their attribute's similarity in reflectance value, colour, size, texture, shape, and pattern (Blaschke *et al*., 2014). The detected segments can be classified by either supervised or rule-based methods (Rizeei *et al*., 2018).

After the pre-processing part, the next stage of OBIA is image segmentation. Quickbird was segmented by multiresolution segmentation (MRS) technique. MRS is a decent optimizing segmentation technique particularly for very-high-resolution satellite imageries, which can minimize average heterogeneity of features while maximizing individual homogeneity using pairwise region merging system (Rizeei *et al*., 2018). The MRS algorithm continually merges image pixels based on textural, spectral, and spatial similarities. Image segmentation is one of the important stages in OBIA because it affects the reliability of the final classified results (Belgiu *et al*., 2014).

MRS has four parameters like shape, compactness, layer weight, and scale that should be supplied with a decent threshold value by expert knowledge based on

the characteristics of target features (Rizeei *et al*., 2019). In this research, the optimal threshold was driven for each MRS parameter by using the trial and error approach after 10-time iterations.

② Classification

The next step of OBIA is deriving the segment's attributes from satellite images. Each segment can be supported from the image by textural, spectral, and geometric attributes. The classification algorithm does classify the segments on the basis of the segment's attributes (Blaschke *et al*., 2014). For this study, we proposed the Dempster-Shafer (DS) algorithm to classify the image segments. DS is one of the recent algorithms that successfully integrated with object-based image analysis where contains defined rules that syndicate numerous belief function values in the same class based on their similarities (Mezaal *et al*., 2018; Rahmati and Melesse, 2016). In order to coordinate the information from diverse classes, DS decently yields the formulated evidence theory (Shafer, 1976). Hence, object evidence is consistently combined to finalize the evaluation of the total evidence. DS can see both imprecision and uncertainty from belief functions, which can compute multiple hypotheses (Rahmati and Melesse, 2016). OBIA-DS classifier is a probability function, which cogitates the most probable segment label from multiple attributes (Mezaal *et al*., 2018; Rizeei *et al*., 2018; Rahmati and Melesse, 2016).

In DS, defined rules were applied to combine the self-determining fragments of evidence into an individual class. The computation is given in Equations 2 and 3:

$$\varphi_{i=1}^{n} m_i(\mathrm{A}) = \frac{1}{1-K} \sum_{\cap_{i=1}^{n} A_n = A} \prod_{i=1}^{n} m_i(A^i) \quad (2)$$

$$K = \sum_{\cap_{i=1}^{n} A_n = \varnothing} \prod_{i=1}^{n} m_i(A^i) \quad (3)$$

where φ signifies the fused constraints and m_i(A) stands for the basic belief assignment (BBA) of subclass A. A^i defines the focal component in respect to data source *i*; while K is the agreement between the fused constraints. Ø also indicates the null set of the equation. Having integrated, a probability indication is developed by the transfer belief model (TBM). A distinctive transfer method is defined in Equation 4:

$$BetP(A_i) = \sum_{A_i \subseteq A_M} \left(\frac{1}{|A_M|}\right) m(A_M) \quad (4)$$

where $BetP(A_i)$ is the transferred Pignistic probability in respect to A_i. The last classification decision is made by choosing those classes with the most similar probability.

Seven LULC classes were recognized to be extracted by OBIA-DS from the study area. For each class enough training and sampling were collected via the stratified random method to avoid any spatial bias caused by clustered training. To evaluate the accuracy of

Table 2. The number of collected GCPs from each class for training and testing of LULC classification process in 2002 and 2015

LULC class	2002			2015		
	Number of Training sites	Number of Testing sites	Total collected GCPs	Number of Training sites	Number of Testing sites	Total collected GCPs
Orchard	64	27	91	55	23	78
Agriculture	34	14	48	25	11	36
Wetland	10	4	14	11	5	15
Wasteland	3	1	4	3	1	4
Building	22	10	32	36	16	52
Road	13	6	19	16	7	23
Water body	5	2	7	5	2	7
Total	151	64	215	151	64	215

classified LULC, overall accuracy and kappa coefficient metrics were applied. To do that, 430 GCPs samples were collected by field surveying to train and test the classification process according to stratified random data collection approach. Technically speaking, 215 GCPs sites were collected in 2002 to classify and assess the LULC 2002 while in 2015 different GCPs but the same number were collected to classify and assess the LULC 2015. 70 percent of total collected samples were used as training to perform the classification and other 30 percent of which were utilized a testing points to evaluate the accuracy of classification. The number of collected GCPs from each class with the associated year are listed in Table 2.

(3) Land use modelling

To implement LTM, it is needed to detect the real changes from 2002 to 2015 at the first stage. Therefore, the classified LULC results from the previous section were analysed to detect their differences. Then According to the detected past trend, the model will anticipate the future scenario of 2030 using artificial neural networks (ANN) technique. There are some parameters known as predictor factors, which can positively impact the predicted LULC growth. Beside those parameters, there is a layer called exclusionary factor that highlights the forbidden area for expansion where do not want to include in predicting analysis (Rizeei *et al*., 2016).

To construct a trustworthy system with enough predictive perspective, ANN ought to be trained by dissimilar input (Pijanowski *et al*., 2014). Training step includes stating input values and adjusting their weights which applied at an individual node by using the learning system. The testing step needs another dataset than the trained network in order to compute the error value self-sufficiently. There are three stages where ANNs engaged in the prediction of LULC change: (i) designing input layers and network based on historical real change, (ii) training the network using proper hidden layer and nodes from clipped inputs, (iii) testing the networks using the entire input dataset

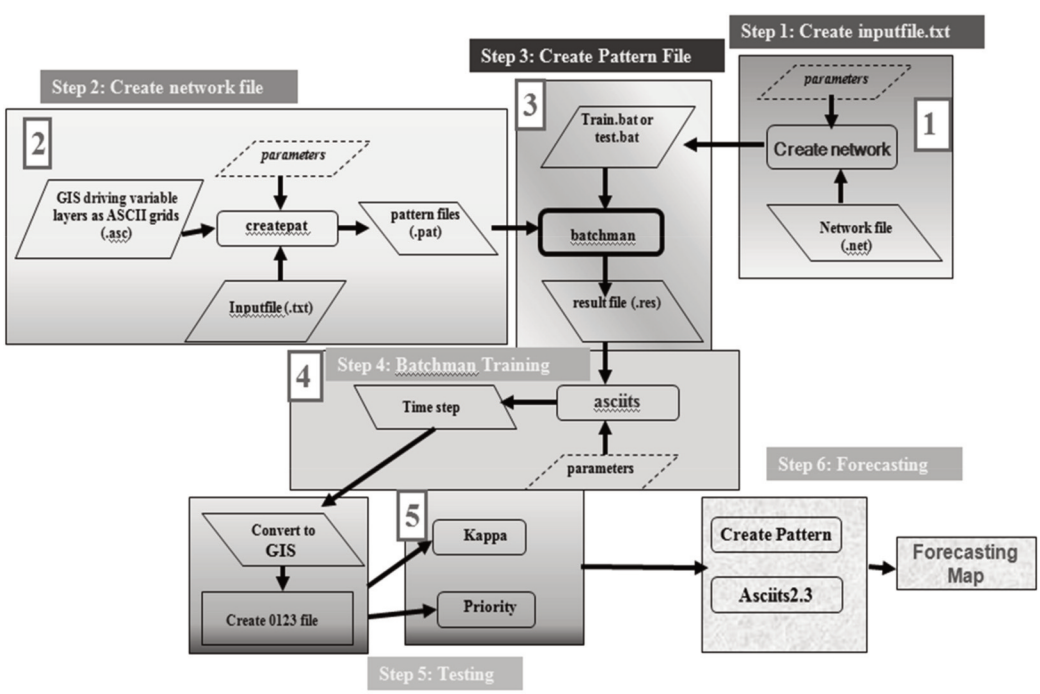

Fig. 2. LTM calculation process integrated with ANN.

(Pijanowski *et al*., 2002; Pijanowski *et al*., 2014).

The LTM results were resulting from five successive phases as shown in Fig. 2. First, data were coded to produce the spatial layers that attach with the predictor factors. Next, connecting the predictors to LCLU changes for all location grids using spatial regulations. Subsequently, ANN implemented to integrate all the grids. After that, all possible scenarios of change were scaled temporally in order to achieve the time sequences for the most probable future of LULC. At the last part the model accuracy was calculated.

The accuracy of predicted LULC can be calculated by comparing Number of cells predicted to change, with Number of cells transitioned to 2030. Percent correct metric (PCM) method can evaluate the accuracy of LTM model to predict the LULC for 2030 as shown in Equation. 5 (Koomen and Borsboom-van Beurden, 2011):

$$PCM = \frac{Number\ of\ cells\ predicted\ to\ change}{\text{Number of cells transitioned to 2030}} \times 100 \quad (5)$$

After implementing all the mentioned procedures, LULC for 2030 was anticipated as Fig. 4 illustrates.

3. Results and discussion

By deploying OBIA-DS method, satellite imagery was classified into seven LULC classes including, road, wetland, waterbody, agriculture, building, orchard, and wasteland. Classification and prediction stages were successfully validated using ground control points (GCPs). The accuracy of the LULC classification was determined using two common accuracy measures (overall and kappa). The overall accuracy for 2002 is 89.5% while for 2015 is 92.4%. Additionally, the accuracy assessment metric of Kappa coefficient indicated 0.87 and 0.91 for 2002 and 2015 classification,

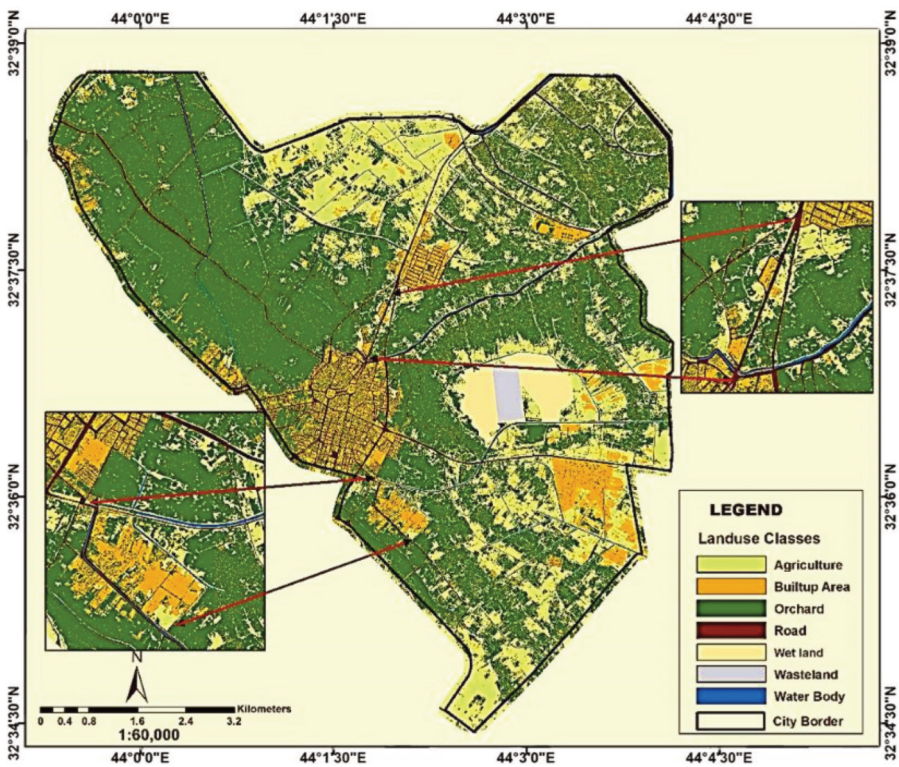

Fig. 3. Extracted LULC for 2002 using OBIA-DS classifier.

respectively.

The building areas were mostly clustered in the city centre while surrounded edges areas were typically covered by orchards and agricultural lands. In 2002, the building area mostly situated at the west and south part of the study area with almost 3382 hectares (Fig. 3). While, in 2015, the building areas located largely at the centre, north, and southeast of the city (Fig. 4). In overall, urbanization has been expanded toward the southeast and north direction almost 993 hectares from 2002 to 2015.

Even by visual interpretation, it is obvious that orchards and agricultural lands have been replaced by urban classes. The growth direction is more from central regions towards the countryside. Most of the countryside urbanizations have taken the place inside orchards where their owners selling these portions to the migrants.

In 2002, more than 50% of the entire study area was covered by orchards areas containing palm dates and other seasonal crops. It was followed by agricultural lands (27%) and building areas (10%). In 2002, however, wastelands and wetland are the smallest LULC classes as 2.2 and 0.6 percentage, respectively. In 2015, the sequence of LULC classes is the same as in 2002, but their percentage was changed dramatically due to urbanization. Orchards area reduced to 42%, agricultural lands shrank down to 21% and building and roads increased up to 26 and 5%, respectively.

1) Change detection and analysis

The trend of LULC changes and urban growth from 2002 to 2015 were assessed using cross-tabulation analysis. The change detection assessment is on the basis of the variation of LULC of thematic maps, which reflects the conversion of each LULC class into others

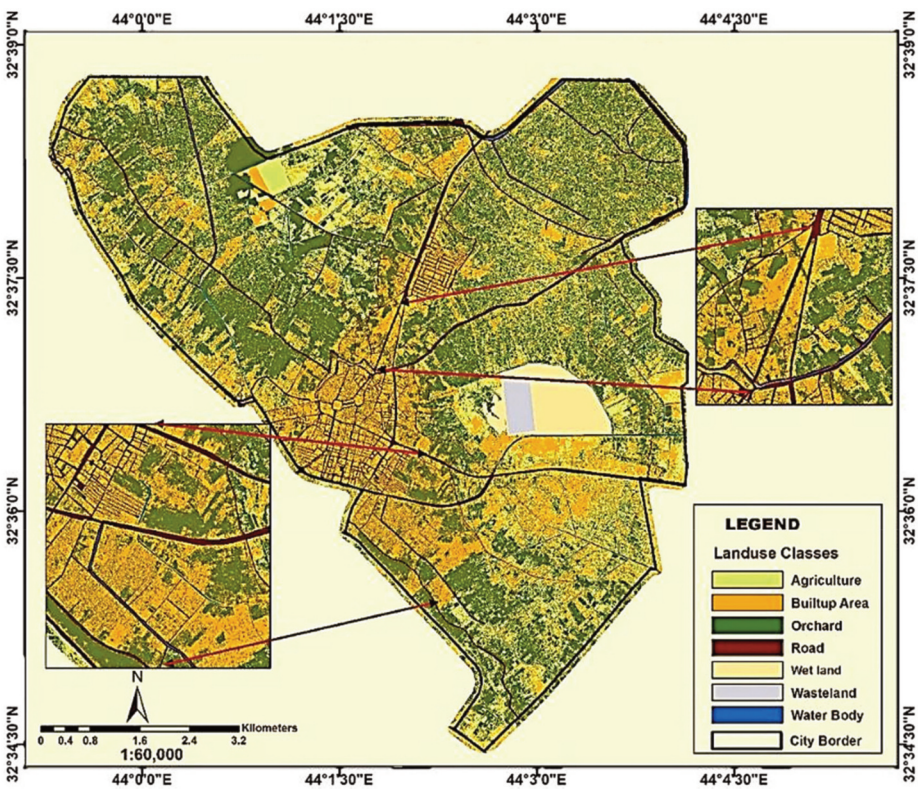

Fig. 4. Extracted LULC for 2015 using OBIA-DS classifier.

over the given time.

The long-term change detection (13-year interval) illustrations that approximately 756 hectares of the orchard and 499 hectares of agricultural lands were replaced by building areas. This growth generally happened toward the centre, southeast, and northwest of the study area. Furthermore, 70 hectares of orchard and agricultural lands converted to the road network. Whilst, 458 hectares of orchard lands were converted into agricultural lands. Nevertheless, wasteland, wetland and water bodies didn't show any substantial changes during these years.

2) Land use prediction analysis

The LULC for 2030 was predicted using LTM method. The prediction was produced with respect to the LULC dynamic trend from 2002 and 2015. This prediction was accomplished to simulate the future trend of urbanization expansion over the study area. The predicted LULC map for 2030 displays the spatial distribution of the seven LULC classes in 2030 (Fig. 5). The overall accuracy for predicted LULC is computed via Equation. 1 as 75.13% with the Kappa index of 0.71. In an argument with other pieces of literature, 60 to 80% is considered an exceptional model for prediction accuracy (Koomen and Borsboom-van Beurden, 2011; Koomen and Stillwell, 2007).

The predicted LULC map shows that in 2030, agriculture and orchard classes would be decreased into by 2233 and 1004 hectares. In other words, the study area will loss 1148 and 694 hectares of orchards and agricultural lands respectively if the trend of urbanization will be continued as the same as 2002 to 2015. While the building area would considerably increase by 1677 hectares from 2002 to 2030. This investigation specifies the city will lose substantial green lands by the year of

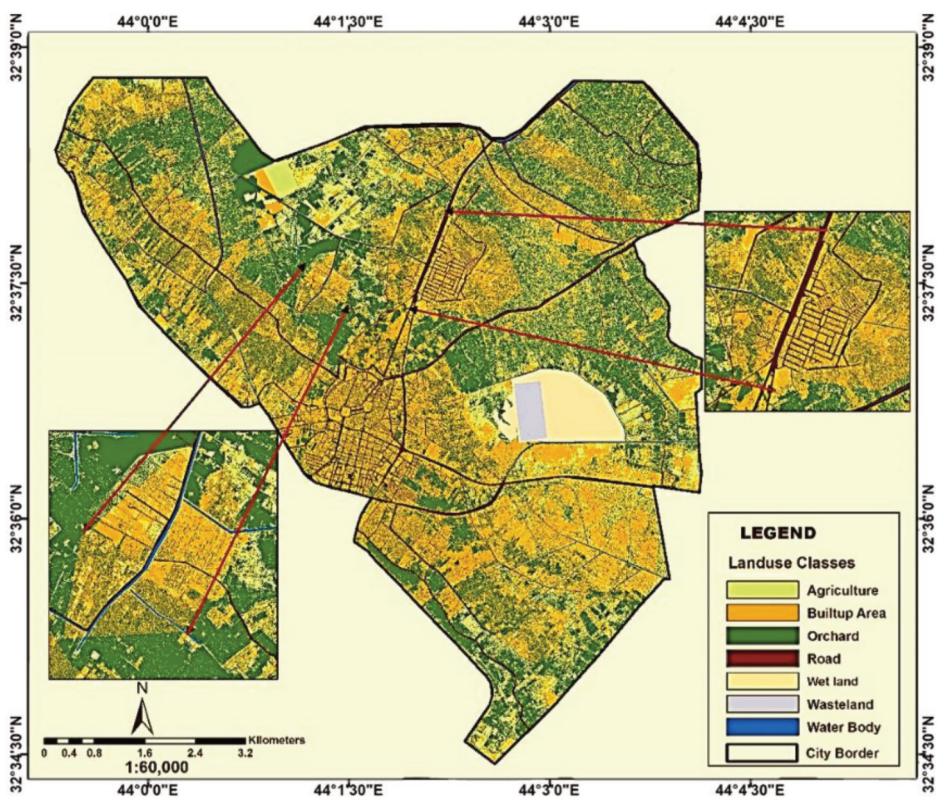

Fig. 5. Predicted LULC for 2030 using LTM technique.

Table 3. Comparative table over extracted and predicted LULC from 2002 to 2030 (Hectare)

LULC class	2002	2015	2030
Orchard	3382.63	2673.53	2233.72
Agriculture	1698.93	1321.37	1004.08
Wetland	137.40	139.63	140.05
Wasteland	39.03	39.43	40.03
Building	658.45	1652.17	2336.01
Road	221.27	322.85	395.95
Water body	110.09	98.84	97.98
Total	6247.82	6247.82	6247.82

2030. As a result, it is vital for Karbala city to make intentional environmental planning to avoid these probable negative consequences. Table 3 and Fig. 6 demonstrate the growth and loss statistics for each LULC class over the 28-year duration.

Fig. 5 reveals probable future transformations would occur in agriculture, orchard, and building areas rather than other classes. The foremost conversion is replacing orchards with built-up areas. Additionally, the prediction scenario confirmed that the expansion of urban development is annually accumulative in the city.

4. Conclusion

The development of sprawl development makes numerous negative issues in terms of social, economic, and environmental sides. This incident can result in not only vanishing valuable natural environments but also creating serious environmental problems due to the lack of appropriate landfill site and sewerage management system. Thus, monitoring and controlling urban growths from remotely sensed datasets can help governments to manage new constructions. We discovered that very high-resolution satellite imagery like Quickbird is an accurate dataset that strongly advisable for urban planning application due to its high temporal and spatial resolution.

This study successfully extracts the LULC, detect

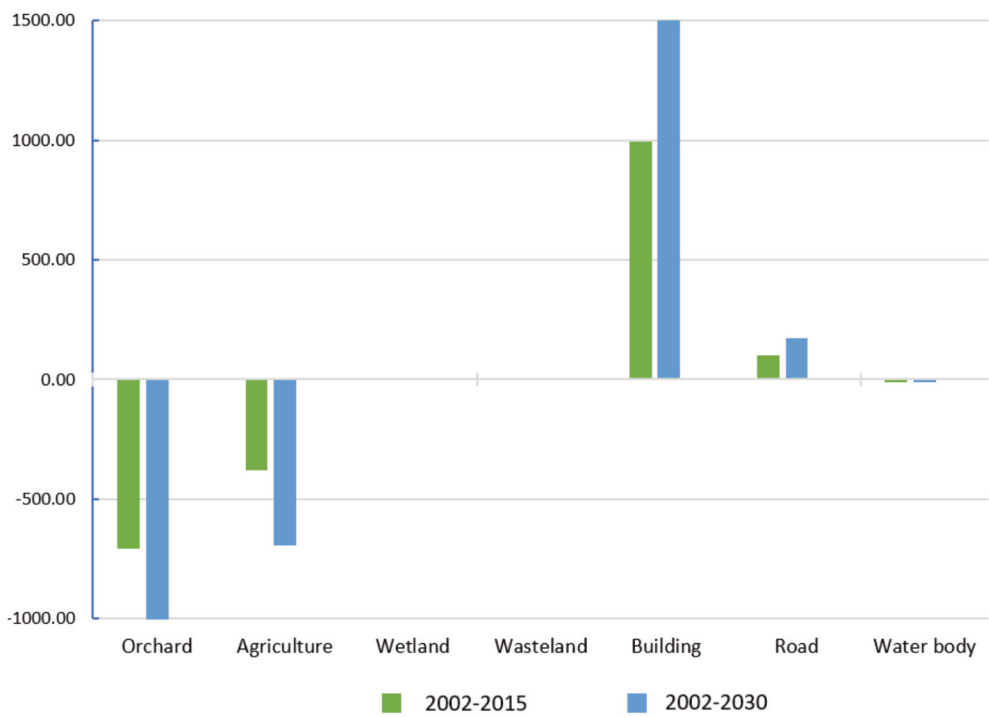

Fig. 6. Graphical chart of positive/negative changes for two given time periods.

the changes, and predict the urban expansion in Karbala city. After pre-processing of Quickbird imagers, seven LULC classes were successfully extracted out. OBIA-DS showed a very high accuracy to classify Quickbird imagers in both years of 2002 and 2015. LTM also presented a promising performance in predicting the LULC future scenarios of 2030 by 75.13% spatial accuracy. The simulation assessment shows a significant growth of urbanization areas that occurred in the orchard and agricultural fields. This investigation specifies the city will lose substantial green lands by the year of 2030. As a result, it is vital for Karbala city to make intentional environmental planning to avoid such probable negative consequences.

Acknowledgements

This work was supported by the Korea Meteorological Administration Research and Development Program under Grant KMI2017-9060.

References

Aal-shamkhi, A. D. S., H. Mojaddadi, B. Pradhan, and S. Abdullahi, 2017. Extraction and modeling of urban sprawl development in Karbala City using VHR satellite imagery, In: Pradhan B. (eds), *Spatial Modeling and Assessment of Urban Form*, Springer, Cham, pp. 281-296.

Abdullahi, S., B. Pradhan, S. Mansor, and A. R. M. Shariff, 2015. GIS-based modeling for the spatial measurement and evaluation of mixed land use development for a compact city, *GIScience & Remote Sensing*, 52(1): 18-39.

Abdullahi, S., B. Pradhan, and H. Mojaddadi, 2018. City compactness: assessing the influence of the growth of residential land use, *Journal of Urban Technology*, 25(1): 21-46.

Belgiu, M., L. Drăguţ, and J. Strobl, 2014. Quantitative evaluation of variations in rule-based classifications of land cover in urban neighbourhoods using WorldView-2 imagery, *ISPRS Journal of Photogrammetry and Remote Sensing*, 87: 205-215.

Bhatta, B., S. Saraswati, and D. Bandyopadhyay, 2010. Urban sprawl measurement from remote sensing data, *Applied Geography*, 30(4): 731-740.

Blaschke, T., G. J. Hay, M. Kelly, S. Lang, P. Hofmann, E. Addink, R. Q. Feitosa, F. van der Meer, H. van der Werff, F. van Coillie, and D. Tiede, 2014. Geographic object-based image analysis–towards a new paradigm, *ISPRS Journal of Photogrammetry and Remote Sensing*, 87: 180-191.

Dadi, D., H. Azadi, F. Senbeta, K. Abebe, F. Taheri, and T. Stellmacher, 2016. Urban sprawl and its impacts on land use change in Central Ethiopia, *Urban Forestry & Urban Greening*, 16: 132-141.

Dietzel, C. and K.C. Clarke, 2007. Toward optimal calibration of the SLEUTH land use change model, *Transactions in GIS*, 11(1): 29-45.

Grimm, V., U. Berger, F. Bastiansen, S. Eliassen, V. Ginot, J. Giske, J. Goss-Custard, T. Grand, S. K. Heinz, G. Huse, A. Huth, J. U. Jepsen, C. Jørgensen, W. M. Mooij, B. Müller, G. Pe'er, C. Piou, S. F. Railsback, A. M. Robbins, M. M. Robbins, E. Rossmanith, N. Rüger, E. Strand, S. Souissi, R. A. Stillman, R. Vabø, U. Visser, and D. L. DeAngelis, 2006. A standard protocol for describing individual-based and agent-based models, *Ecological Modelling*, 198(1-2): 115-126.

He, C., P. Shi, D. Xie, and Y. Zhao, 2010. Improving the normalized difference built-up index to map urban built-up areas using a semiautomatic segmentation approach, *Remote Sensing Letters*, 1(4): 213-221.

Koomen, E. and J. Borsboom-van Beurden, 2011.

Land-use modelling in planning practice, Springer Science & Business Media, Berlin, Germany, vol. 101.

Koomen, E. and J. Stillwell, 2007. *Modelling Land-Use change*, Springer, Dordrecht, Netherlands, pp. 1-22.

Kumar, A., A. C. Pandey, and A. Jeyaseelan, 2012. Built-up and vegetation extraction and density mapping using WorldView-II, *Geocarto International*, 27(7): 557-568.

Li, X. and A. G.-O. Yeh, 2000. Modelling sustainable urban development by the integration of constrained cellular automata and GIS, *International Journal of Geographical Information Science*, 14(2): 131-152.

Mezaal, M., B. Pradhan, and H. Rizeei, 2018. Improving Landslide Detection from Airborne Laser Scanning Data Using Optimized Dempster–Shafer, *Remote Sensing*, 10(7): 1029.

Rizeei, H. M., B. Pradhan, and M. A. Saharkhiz, 2019. Urban object extraction using Dempster Shafer feature-based image analysis from worldview-3 satellite imagery, *International Journal of Remote Sensing*, 40(3): 1092-1119.

Nampak, H., B. Pradhan, H. M. Rizeei, and H. J. Park, 2018. Assessment of land cover and land use change impact on soil loss in a tropical catchment by using multitemporal SPOT–5 satellite images and R evised U niversal Soil L oss E quation model, *Land Degradation & Development*, 29(10): 3440-3455.

Pijanowski, B. C., D. G. Brown, B. A. Shellito, and G. A. Manik, 2002. Using neural networks and GIS to forecast land use changes: a land transformation model, *Computers, Environment and Urban Systems*, 26(6): 553-575.

Pijanowski, B. C., A. Tayyebi, J. Doucette, B. K. Pekin, D. Braun, and J. Plourde, 2014. A big data urban growth simulation at a national scale: configuring the GIS and neural network based land transformation model to run in a high performance computing (HPC) environment, *Environmental Modelling & Software*, 51: 250-268.

Pontius Jr, R.G. and H. Chen, 2006. *GEOMOD modeling*, Clark University, Worcester, MA, USA.

Rahmati, O. and A. M. Melesse, 2016. Application of Dempster–Shafer theory, spatial analysis and remote sensing for groundwater potentiality and nitrate pollution analysis in the semi-arid region of Khuzestan, Iran, *Science of The Total Environment*, 568: 1110-1123.

Rizeei, H. M. and B. Pradhan, 2019. Urban Mapping Accuracy Enhancement in High-Rise Built-Up Areas Deployed by 3D-Orthorectification Correction from WorldView-3 and LiDAR Imageries, *Remote Sensing*, 11(6): 692.

Rizeei, H. M., M. A. Saharkhiz, B. Pradhan, and N. Ahmad, 2016. Soil erosion prediction based on land cover dynamics at the Semenyih watershed in Malaysia using LTM and USLE models, *Geocarto International*, 31(10): 1158-1177.

Rizeei, H. M., H. Z. Shafri, M. A. Mohamoud, B. Pradhan, and B. Kalantar, 2018. Oil palm counting and age estimation from WorldView-3 imagery and LiDAR data using an integrated OBIA height model and regression analysis, *Journal of Sensors*, vol. 2018, Article ID 2536327, https://zdoi.org/10.1155/2018/2536327.

Shafer, G., 1976. *A mathematical theory of evidence*, Princeton University Press, Princeton, NJ, USA, vol. 42.

Sridharan, H., 2012. *Object-based approaches to image classification for hyperspatial and hyperspectral data*, The University of Texas at Dallas, Richardson, TX, USA.

Tayyebi, A., B. K. Pekin, B. C. Pijanowski, J. D. Plourde, J. S. Doucette, and D. Braun, 2013. Hierarchical modeling of urban growth across the conterminous

USA: developing meso-scale quantity drivers for the Land Transformation Model, *Journal of Land Use Science*, 8(4): 422-442.

Verburg, P.H., W. Soepboer, A. Veldkamp, R. Limpiada, V. Espaldon, and S.S. Mastura, 2002. Modeling the spatial dynamics of regional land use: the CLUE-S model, *Environmental Management*, 30(3): 391-405.